NASA/TM–1999–104606, Vol. 15

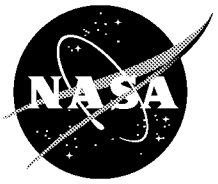

Technical Report Series on Global Modeling and Data Assimilation

Max J. Suarez, Editor

Volume 15

A Solar Radiation Parameterization for Atmospheric Studies

Ming-Dah Chou and Max J. Suarez

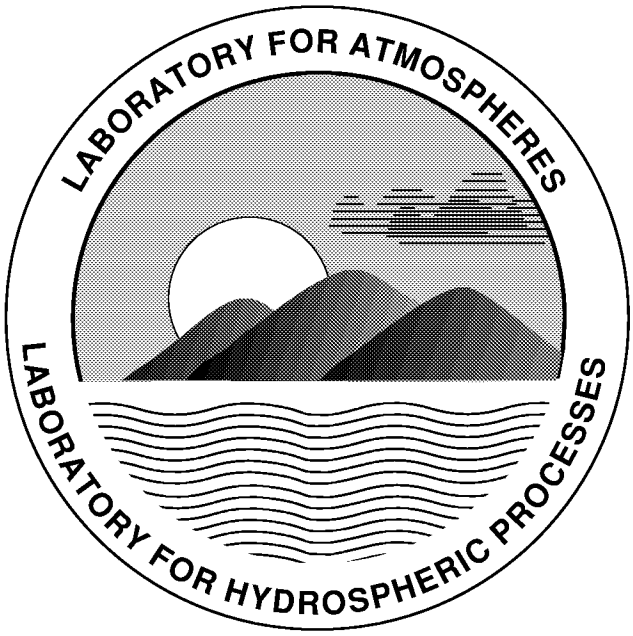

Climate and Radiation Branch
NASA Seasonal to Interannual Prediction Project

June 1999

The NASA STI Program Office … in Profile

Since its founding, NASA has been dedicated to the advancement of aeronautics and space science. The NASA Scientific and Technical Information (STI) Program Office plays a key part in helping NASA maintain this important role.

The NASA STI Program Office is operated by Langley Research Center, the lead center for NASA's scientific and technical information. The NASA STI Program Office provides access to the NASA STI Database, the largest collection of aeronautical and space science STI in the world. The Program Office is also NASA's institutional mechanism for disseminating the results of its research and development activities. These results are published by NASA in the NASA STI Report Series, which includes the following report types:

- TECHNICAL PUBLICATION. Reports of completed research or a major significant phase of research that present the results of NASA programs and include extensive data or theoretical analysis. Includes compilations of significant scientific and technical data and information deemed to be of continuing reference value. NASA's counterpart of peer-reviewed formal professional papers but has less stringent limitations on manuscript length and extent of graphic presentations.
- TECHNICAL MEMORANDUM. Scientific and technical findings that are preliminary or of specialized interest, e.g., quick release reports, working papers, and bibliographies that contain minimal annotation. Does not contain extensive analysis.
- CONTRACTOR REPORT. Scientific and technical findings by NASA-sponsored contractors and grantees.
- CONFERENCE PUBLICATION. Collected papers from scientific and technical conferences, symposia, seminars, or other meetings sponsored or cosponsored by NASA.
- SPECIAL PUBLICATION. Scientific, technical, or historical information from NASA programs, projects, and mission, often concerned with subjects having substantial public interest.
- TECHNICAL TRANSLATION. English-language translations of foreign scientific and technical material pertinent to NASA's mission.

Specialized services that complement the STI Program Office's diverse offerings include creating custom thesauri, building customized databases, organizing and publishing research results . . . even providing videos.

For more information about the NASA STI Program Office, see the following:

- Access the NASA STI Program Home Page at http://www.sti.nasa.gov/STI-homepage.html
- E-mail your question via the Internet to help@sti.nasa.gov
- Fax your question to the NASA Access Help Desk at (301) 621-0134
- Telephone the NASA Access Help Desk at (301) 621-0390
- Write to:
  NASA Access Help Desk
  NASA Center for AeroSpace Information
  7121 Standard Drive
  Hanover, MD 21076–1320

NASA/TM–1999–104606, Vol. 15

Technical Report Series on Global Modeling and Data Assimilation

Max J. Suarez, Editor
Goddard Space Flight Center, Greenbelt, Maryland

Volume 15

A Solar Radiation Parameterization for Atmospheric Studies

Ming-Dah Chou
Max J. Suarez

Goddard Space Flight Center
Greenbelt, Maryland

National Aeronautics and
Space Administration

Goddard Space Flight Center
Greenbelt, Maryland 20771

June 1999

Available from:

NASA Center for AeroSpace Information
7121 Standard Drive
Hanover, MD 21076–1320
Price Code: A17

National Technical Information Service
5285 Port Royal Road
Springfield, VA 22161
Price Code: A10

Abstract

This NASA Technical Memorandum documents the solar radiative transfer model (CLIRAD-SW) developed at the Goddard Climate and Radiation Branch, which has been applied to various atmospheric models used in the Goddarad Laboratory for Atmospheres, including a general circulation model, a mesoscale model, and a cloud ensemble model. It includes the absorption due to water vapor, O_3, O_2, CO_2, clouds, and aerosols. Interactions among the absorption and scattering by clouds, aerosols, molecules (Rayleigh scattering), and the surface are fully taken into account. Fluxes are integrated virtually over the entire spectrum, from 0.175 μm to 10 μm.

Depending upon the nature of absorption, different approaches are applied to different absorbers. In the ultraviolet (UV) and photosynthetically active (PAR) region, the spectrum is divided into 8 bands, and single O_3 absorption coefficient and Rayleigh scattering coefficient are used for each band. In the infrared, the spectrum is divided into 3 bands, and the k-distribution method is applied. Ten absorption coefficients are used in each band. The flux reduction due to O_2 is derived from a simple function, while the flux reduction due to CO_2 is derived from precomputed tables.

Reflection and transmission of a cloud and aerosol-laden layer are computed using the δ-Eddington approximation. Fluxes are then computed using the two-stream adding approximation. For a cloud layer, the optical thickness is parameterized as a function of cloud water/ice amount and the effective particle size, whereas the single-scattering albedo and asymmetry factor are parameterized as a function of the effective particle size. The parameterizations are applied separately to water and ice particles. A maximum-random approximation is adopted for the overlapping of clouds at different heights. Aerosol optical properties are specified input parameters to the radiation model.

A special feature of this model is that absorption due to a number of minor absorption bands is included. Individually the absorption in those minor bands is small, but collectively the effect is large, ~10 % of the atmospheric heating. Integrated over all spectral bands and all absorbers, the surface heating is computed accurately to within a few watts per meter squared of high spectral-resolution calculations, and the atmospheric heating rate between 0.01 hPa and the surface is accurate to within 5%.

A complete computer code of the CLIRAD-SW model with sample calculations is available at http://climate.gsfc.nasa.gov/~chou/clirad_sw

TABLE OF CONTENTS

List of Figures

List of Tables

1. INTRODUCTION

Solar radiation is the ultimate source of energy for the Earth's climate. A small error in heating rate calculations might induce large errors in model-simulated climate. It is very important that solar heating is calculated accurately in an atmospheric model, not only for the total heating but also for the horizontal and vertical distributions of the heating. One of the major difficulties in the calculation of atmospheric radiative heating is that it requires a huge amount of computing time using detailed spectral and angular integrations. There are tens of thousands of molecular lines across the spectrum. The half-width of a line is ~0.05 cm^{-1} in the troposphere, which is much narrower than the mean spacing of lines. As a result, the absorption coefficient varies rapidly with wavenumbers. Detailed spectral integration of radiative transfer requires $>10^6$ spectral points. When scattering due to clouds and aerosols is involved, angular integration becomes the major computational burden. Adding to the complexity of the radiative transfer calculations are the overlapping of absorption due to multiple absorbers, the overlapping of clouds at various heights, and the wide ranges of cloud microphysical and optical properties.

There are several solar radiation parameterizations with various complexities available for use in atmospheric models (Fouquart et al., 1991 and the references therein). At the NASA/Goddard Space Flight Center, Climate and Radiation Branch, we have developed a model for solar radiative transfer, which can be traced back at least to the past 10 years. Depending upon the spectral properties of absorbers and scatterers, as well as the heights where heating is important, various parameterizations are applied. This model has been applied to the various atmospheric model used in the Goddarad Laboratory for Atmospheres, which include a general circulation model (Koster and Suarez, 1995), a mesoscale model, and a cloud ensemble model (Tao et al., 1996). This NASA Technical Memorandum documents the detailed treatment of the solar radiative transfer in the model.

2. SPECTRAL BANDS

Table 1 shows the spectral bands of the solar radiation model. There are eight bands in the ultraviolet and visible region ($\nu>14280$ cm^{-1}) and three bands in the infrared region ($\nu<14280$ cm^{-1}). Also shown in the table are the absorbers and scatterers included in the calculation of solar fluxes in each band, as well as the equations used for computing the

Table 1. Gaseous absorption and Rayleigh scattering in the broadband radiation parameterizations and the equations used for transmittance and flux calculations. Clouds and aerosols are included in all bands.

Band	Spectral Range (cm^{-1})	Spectral Range (μm)	Absorber/ Scatterer	Equation
1	(44440-57140)	(0.175-0.225)	O_3	3.12
			Rayleigh	--
2	(40820-44440 35700-38460)	(0.225-0.245 0.260-0.280)	O_3	3.12
			Rayleigh	--
3	(38460-40820)	(0.245-0.260)	O_3	3.12
			Rayleigh	--
4	(33900-35700)	(0.280-0.295)	O_3	3.12
			Rayleigh	--
5	(32260-33900)	(0.295-0.310)	O_3	3.12
			Rayleigh	--
6	(31250-32260)	(0.310-0.320)	O_3	3.12
			Rayleigh	--
7	(25000-31250)	(0.320-0.400)	O_3	3.12
			Rayleigh	--
8	(14280-25000)	(0.400-0.700)	O_3	3.12
			H_2O	3.12
			Rayleigh	--
9	(8200-14280)	(0.70-1.22)	H_2O	3.11
			O_3*	3.12
			Rayleigh	--
10	(4400-8200)	(1.22-2.27)	H_2O	3.11
			Rayleigh	--
11	(1000-4400)	(2.27-10.0)	H_2O	3.11
	Total Spectrum		O_2	3.16
	Total Spectrum		CO_2	3.19; 3.24

* O_3 absorption is folded into Band 8

transmission function. The first eight bands involves the O_3 absorption and Rayleigh scattering. Band 8 also includes the weak absorption due to water vapor. Single values of the O_3 absorption coefficient, the water vapor absorption coefficient, and Rayleigh scattering coefficient are used in each of the 8 bands. Bands 9-11 include the water vapor absorption and Rayleigh scattering. Water vapor absorption in these bands is significant, and the k-distribution method is used. Band 9 also includes the weak O_3 absorption. The O_3 absorption in this band is folded into the absorption in Band 8. The absorption due to O_2 and CO_2 is of secondary importance but occur in wide spectral ranges. Different approaches which compute only the reduction in fluxes are used. Clouds and aerosols are included in all bands.

3. GASEOUS ABSORPTION

3.1 High spectral-resolution calculations

The absorption coefficients of water vapor, O_2, and CO_2 vary rapidly with wavenumber. Parameterizations for the absorption due to these gases are based on line-by-line calculations using the latest (1996) version of the molecular line parameters compiled at AFGL (Rothman, 1987). The shape of an absorption line is assumed to follow the Voigt function. The Voigt half-width is a function of pressure, temperature and wavenumber. Because the shape of the far wings of a line is not well known, the absorption coefficient of a molecular line is set to zero at wavenumbers >10 cm^{-1} from the line center. The spectral resolution of the line-by-line calculations is 0.002 cm^{-1}, which is adequate for solar flux calculations. The O_3 absorption coefficient varies by several orders of magnitude in the UV and visible regions but rather smoothly with wavenumber. Absorption due to O_3 is computed with a resolution of ~0.003 μm. The absorption coefficient is interpolated from the spectral values given in WMO (1985). The effect of pressure and temperature on the O_3 absorption is small and, hence, neglected.

3.2 The k-distribution method

The width of an absorption line of water vapor, O_2 , or CO_2 is much smaller than the average spacing between absorption lines. It decreases linearly with decreasing pressure and is only ~0.05 cm^{-1} in the lower troposphere. As a result, the absorption coefficient varies rapidly within narrow spectral intervals, and accurate radiative transfer calculations require a

high spectral resolution. For the case of water vapor absorption, the high resolution line-by-line method requires flux calculations at $>10^6$ spectral points. For an atmospheric layer where temperature θ and pressure p can be assumed constant, the wavenumbers with the same absorption coefficient are radiatively identical and can be treated as one entity. Fluxes at those wavenumbers with the same absorption coefficient need to be computed only once. Therefore, flux calculations can be greatly simplified by grouping the wavenumbers with the same absorption coefficient. Within a small interval $\delta\nu$ where the spectral variation of insolation (incoming solar radiation) is small, the integration of fluxes over wavenumbers can be replaced by that over the absorption coefficient. The mean transmission function of the interval $\delta\nu$ can be written as

$$T(w') = \int_{\delta\nu} e^{-k_\nu(p,\theta)w'} d\nu / \delta\nu = \int_0^\infty e^{-kw'} g(k;p,\theta)dk \approx \sum_{i=1}^{n} a_i(p,\theta) e^{-k_i w'} \qquad (3.1)$$

where w' is the absorber amount, k_ν is the absorption coefficient at the wavenumber ν, g is the k-distribution density function (cf. Arking and Grossman, 1972) such that the fraction of spectrum with the absorption coefficient between $k - dk/2$ and $k + dk/2$ is $g(k)dk$, and a_i $[= g(k_i)\Delta k_i]$ is the k-distribution function. Chou and Lee (1996) has shown that the k-distribution method requires only 10 values of k (i.e. n=10) for accurate calculations of solar heating due to water vapor using the k-distribution method, instead of $>10^6$ spectral points using the line-by-line method.

In the atmosphere where pressure and temperature change with height, the wavenumbers with a common absorption coefficient at a given height will not necessarily have a common absorption coefficient at other heights. These wavenumbers are no longer radiatively identical, and the k-distribution method cannot be used without applying assumptions. Pressure affects the width of a molecular line. Near the center of a line, the absorption is strong, and flux calculations are not sensitive to errors in the absorption coefficient. Distant from line centers, the absorption coefficient varies nearly linearly with pressure. On the other hand, temperature affects absorption primarily through its effect on the line intensity, which is constant for a given line. Thus, the temperature effect on absorption is rather smooth with respect to wavenumber. It has been shown by Chou (1986) that fluxes can be calculated accurately using the one-parameter scaling for the absorption coefficient,

$$k_\nu(p,\theta) = k_\nu(p_r,\theta_r)\left(\frac{p}{p_r}\right)^m f(\theta,\theta_r) \tag{3.2}$$

where p_r is the reference pressure, θ_r is the reference temperature, $m \le 1$, and $f(\theta,\theta_r)$ is the temperature scaling function. As explained in Chou (1986), the optical path between the top of the atmosphere and the middle and lower troposphere is large near the center of absorption lines. It follows that solar fluxes in the middle and lower troposphere are primarily attributable to the spectral intervals between absorption lines, and the wing-approximation of (3.2) can be applied to accurately compute fluxes. In the stratosphere, the solar heating due to water vapor and O_2 is small, and underestimation of the absorption coefficient induced by the use of (3.2) does not have a significant effect on the heating rate. In the upper troposphere, the absorption is neither strong nor weak, and the error induced by the scaling is expected to have a large impact on flux calculations. However, if we choose p_r to be the upper tropospheric pressure, then $p / p_r \approx 1$ in the upper troposphere, and the scaling introduces only a small error in the absorption coefficient. It has been found (Chou, 1986) that the solar fluxes can be computed accurately by choosing p_r=300 hPa and m=0.8. Flux calculations are not sensitivity to m for 0.7<m<0.9. The effect of temperature on the absorption of solar radiation is weak. For the absorption due to water vapor, it is approximated by

$$f(\theta,\theta_r) = 1 + 0.00135(\theta - \theta_r) \tag{3.3}$$

where θ_r=240 K. For the absorption due to O_2, and CO_2, the temperature effect is neglected, i.e. $f(\theta,\theta_r)$=1.

Using the scaling of (3.2), Equation (3.1) becomes

$$T(w) = \sum_{i=1}^{n} a_i(p_r,\theta_r)e^{-k_i w} \tag{3.4}$$

where

$$w(p,\theta) = w'\left(\frac{p}{p_r}\right)^m f(\theta,\theta_r) \tag{3.5}$$

Thus, the scaling of the absorption coefficient is reduced to the scaling of the absorber amount. The mean transmission given in (3.4) is independent of wavenumber, and flux calculations are greatly simplified. It is noted that the physical basis for the k-distribution

method with the one-parameter pressure and temperature scaling is the same as for the correlated k-distribution method (Wang and Ryan, 1983; Goody et al., 1989; Lacis and Oinas, 1991; Fu and Liou, 1992; Mlawer et al., 1997), i.e., the dominant effect of line wings on the absorption. The correlated k-distribution method correlates the values of k at different pressure and temperature through table look-up. The k-distribution method with the one-parameter scaling correlates values of k through (3.2). The accuracies of these two approaches are comparable, but the latter is much simpler than the former.

3.3 Absorption due to water vapor in the infrared (Bands 9-11)

Figure 1a shows the spectral distribution of the water vapor transmission function of the entire atmospheric column in the vertical direction averaged over 10 cm^{-1}. The atmosphere used is typical of mid-latitude summer conditions (Anderson et al., 1986). It shows that water vapor absorption varies strongly with wavenumber. The k-distribution method is used to parameterize water vapor absorption. For a spectral band with a width $\Delta\nu$, the direct solar flux at a given pressure level p can be written as

$$F(w) = \int_{\Delta\nu} e^{-k_\nu w} S_\nu d\nu \tag{3.6}$$

where S_ν is the extraterrestrial solar flux density at the wavenumber ν multiplied by the cosine of the solar zenith angle, k is the absorption coefficient at p_r and θ_r, and w is the scaled absorber amount, given by (3.5), above the pressure level p and in the direction of the solar beam. The flux-weighted mean transmission of a band is given by

$$T(w) = \int_{\Delta\nu} e^{-k_\nu w} S_\nu d\nu \Big/ \int_{\Delta\nu} S_\nu d\nu \tag{3.7}$$

If we divide a spectral band into m small intervals and apply the k-distribution method of (3.4), Equation (3.6) becomes

$$F(w) = \sum_{j=1}^{m} S_j \left[\int_{\Delta\nu_j} e^{-k_\nu w} d\nu \right] = \sum_{i=1}^{n} \left[\sum_{j=1}^{m} a_{i,j} S_j \Delta\nu_j \right] e^{-k_i w} \tag{3.8}$$

where S_j is the mean flux density at the top of the atmosphere in the interval $\Delta\nu_j$, $a_{i,j}$ is the k-distribution function in the spectral interval $\Delta\nu_j$, n is number of k-intervals, and

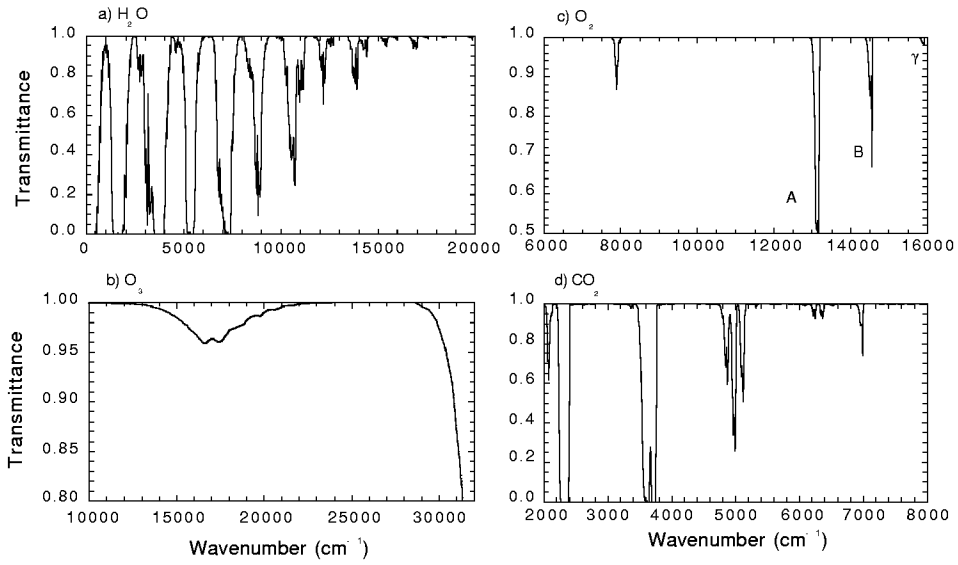

Figure 1. Spectral distribution of the transmission function of the entire column of a mid-latitude summer atmosphere in the vertical direction averaged over 10 cm^{-1} for water vapor, O_3, O_2, and CO_2.

$$\Delta\nu = \sum_{j=1}^{m} \Delta\nu_j \tag{3.9}$$

By defining

$$h_i = \sum_{j=1}^{m} a_{i,j} S_j \Delta\nu_j / S_o \tag{3.10}$$

which is the flux-weighted k-distribution function at p_r=300 hPa and θ_r=240 K, Equation (3.8) becomes

$$F(w) = S_o \sum_{i=1}^{n} h_i e^{-k_i w} \tag{3.11}$$

where S_o is the total insolation at the top of the atmosphere (=extraterrestrial solar flux multiplied by the cosine of the solar zenith angle). Equation (3.11) is applied to compute the

water vapor transmission function in the infrared (Bands 9-11). Fluxes are computed for each k_i, and the total flux is the sum of these fluxes weighted by the k-distribution function. Table 2 gives the values of k and the k-distribution function used in the three IR bands. It is noted that if n is smaller than 10, say, 7, the calculated heating rate profile will oscillate strongly with height, as shown in Figure 1 of Chou and Lee (1996). It is also noted that the reason for dividing the infrared into three bands is the large change with wavenumber in the cloud and aerosol optical thickness and single-scattering albedo.

Table 2. The flux-weighted k-distribution function of water vapor, h, in the infrared for p_r=300 hPa and θ_r=240 K. Sum of all h values is 0.52926. The unit of the absorption coefficient, k, is g^{-1} cm^2.

k-Interval	k	h (Band 9)	h (Band 10)	h (Band 11)
1	0.0010	0.20673	0.08236	0.01074
2	0.0133	0.03497	0.01157	0.00360
3	0.0422	0.03011	0.01133	0.00411
4	0.1334	0.02260	0.01143	0.00421
5	0.4217	0.01336	0.01240	0.00389
6	1.3340	0.00696	0.01258	0.00326
7	5.6230	0.00441	0.01381	0.00499
8	31.620	0.00115	0.00650	0.00465
9	177.80	0.00026	0.00244	0.00245
10	1000.0	0.00000	0.00094	0.00145

3.4 Absorption due to water vapor in the PAR region (Band 8)

The absorption due to water vapor in the photosynthetically active radiation (PAR) region between 14280 cm^{-1} and 25000 cm^{-1} (Band 8) is weak (Figure 1a), and the mean transmission defined by (3.7) can be approximated by

$$T(w) \approx \int_{\Delta\nu} (1 - k_\nu w) S_\nu d\nu \Big/ \int_{\Delta\nu} S_\nu d\nu = 1 - \bar{k} w \approx e^{-\bar{k} w} \tag{3.12}$$

where $\bar{k}$ is an effective absorption coefficient, and w is the scaled water vapor amount given by (3.5). Using the line-by-line method, the mean transmission function $T(w)$ given by (3.7) is first computed at 300 hPa and 240 K for a large range of w. For each w, an effective absorption coefficient is then computed by inverting (3.12),

$$\bar{k}(w) = -\frac{1}{w} \ln T(w) \tag{3.13}$$

The value of $\bar{k}$ is found to range from 0.00065 to 0.00080 g^{-1} cm^2, and a mean value of 0.00075 g^{-1} cm^2 is used to compute the water vapor absorption in Band 8 from (3.12).

3.5 Absorption due to O_3 in the UV and PAR regions (Bands 1-8)

The eight bands in UV and PAR spectral regions as shown in Table 1 are relatively narrow. The range of the O_3 absorption coefficient in each band is small and the mean transmission function can also be approximated by (3.12). By dividing the UV and PAR regions into 127 narrow bands with a width of ~0.003 μm and using the O_3 absorption coefficient given in WMO (1986), the mean O_3 transmission function is computed from (3.7). The same procedures described above for the determination of the effective water vapor absorption coefficient is applied to derive the effective O_3 absorption coefficient, which is given in Table 3. It is noted that the effect of temperature and pressure on the O_3 absorption

Table 3. The spectral range, fractional solar flux, effective ozone and water vapor absorption coefficients, and Rayleigh scattering coefficient. Sum of S / S_o is 1.

	Band	S / S_o	O_3 Absorption Coefficient $(cm\text{-}atm)^{-1}$	H_2O Absorption Coefficient $(g^{-1}\ cm^2)$	Ray. Scattering Coefficient (hPa^{-1})
UV-C					
	1	0.00057	30.47		0.00604
	2	0.00367	187.24		0.00170
	3	0.00083	301.92		0.00222
UV-B					
	4	0.00417	42.83		0.00132
	5	0.00600	7.09		0.00107
	6	0.00556	1.25		0.00091
UV-A					
	7	0.05913	0.0345		0.00055
PAR					
	8	0.39081	0.0572*	0.00075	0.00012
Near IR					
	9	0.32055		See Table 2	0.0000156
	10	0.16536		See Table 2	0.0000018
	11	0.04335		See Table 2	0.0

* Enhanced by the O_3 absorption in Band 9.

is small, and the one-parameter scaling is not applied to the O_3 amount. Also shown in the table is the ratio of the extraterrestrial solar radiation of each band to that of the total spectrum, S / S_o. Equation (3.12) is applied to compute the transmission due to O_3 in Bands 1-8.

3.6 Absorption due to O_3 in the infrared

As shown in Figure 1b, the absorption due to ozone in the near infrared (Band 9) is restricted to a narrow spectral region next to Band 8 where absorption due to water vapor is weak. However, the absorption due to water vapor in the rest of Band 9 is not necessarily weak. Thus, calculations of the ozone heating in the near infrared would require adding another band in the broadband radiation model. Because the absorption due to water vapor and O_3 is weak in Band 8, the O_3 absorption in Band 9 can be folded into the absorption in Band 8 as if it were the absorption due to another absorber. To do so, the effective O_3 absorption coefficient of Band 8, $\overline{k_8}$, is replaced by

$$\overline{k} = \overline{k_8} + \Delta k \tag{3.14}$$

where Δk satisfies

$$\left(1 - e^{-\Delta k w'}\right) \int_{\Delta\nu_8} S_\nu d\nu = \int_{\Delta\nu_9} \left(1 - e^{-k_\nu w'}\right) S_\nu d\nu \tag{3.15}$$

so that the absorption of solar radiation due to O_3 in the near infrared is correctly computed, where w' is the ozone amount, and $\Delta\nu_8$ and $\Delta\nu_9$ are the widths of Bands 8 and 9, respectively. For a wide range of w' found in the atmosphere, the value of Δk ranges between 0.0032 and 0.0033 $(\text{cm-atm})_{\text{STP}}^{-1}$. Therefore, the ozone absorption coefficient in Band 8 is enhanced by 0.0033 $(\text{cm-atm})_{\text{STP}}^{-1}$ to take into account the absorption by ozone in the infrared. The O_3 absorption coefficient of Band 8 given in Table 3 includes this extra absorption. This approach to computing the ozone absorption in the near infrared requires no extra computing time.

3.7 Absorption due to O_2

The absorption due to O_2 occurs in narrow spectral intervals, but is not necessary weak near band centers (Figure 1c). Using the line-by-line method, Chou (1990) computed the

mean O_2 transmission function in the A and B bands centered at 13150 cm^{-1} and 14510 cm^{-1} and fit the transmission function by a square-root approximation,

$$T(w) = e^{-\bar{k}\sqrt{w}} \tag{3.16}$$

The absorption in the weak bands centered at 7890 cm^{-1} and 15870 cm^{-1} was not included. To include the absorption in all those bands, the mean transmission function of O_2 at p_r=300 hPa and θ_r=240 K in the spectral regions 7600-8050, 12850-13190, 14310-14590, and 15730-15930 cm^{-1} is computed from (3.7) using the line-by-line method, and the effective mean absorption coefficient $\bar{k}$ is computed from

$$\bar{k}(w) = -\frac{1}{\sqrt{w}} \ln T(w) \tag{3.17}$$

The value of $\bar{k}$ varies between 0.000135 $(\text{cm-atm})_{STP}^{-1/2}$ and 0.000155 $(\text{cm-atm})_{STP}^{-1/2}$ for a large range of the scaled O_2 amount, w, encountered in the atmosphere. A mean value of 0.000145 $(\text{cm-atm})_{STP}^{-1/2}$ is used in the broadband radiation model.

The O_2 absorption bands are located between water vapor absorption bands. Thus, water vapor has little effect on the solar heating due to O_2. Instead of computing fluxes in the O_2 bands, the reduction in fluxes due to O_2 absorption is computed from

$$\Delta F(w) = S\left(1 - e^{-\bar{k}\sqrt{w}}\right) \tag{3.18}$$

The insolation, S, in the spectral regions 7600-8050, 12850-13190, 14310-14590, and 15730-15930 cm^{-1} is 6.33% of the total solar flux at the top of the atmosphere.

The O_2 transmission function, Equation (3.16), is similar to that used by Kiehl and Yamanouchi (1985), except the pressure scaling of (3.5) is different. It is band-averaged, does not follow Beer's law, and, hence, cannot be applied to the δ-Eddington approximation for multiple-scattering calculations. We apply (3.16) only to clear atmospheres. For cloudy atmospheres, a simple scaling approach is used to compute the O_2 heating, which is addressed in Section 6.4.

3.8 Absorption due to CO_2

The absorption due to CO_2 is small but overlaps significantly with the absorption due to water vapor in certain spectral regions (Figures 1a and 1d). By assuming that CO_2 heating in the stratosphere is not important, Chou (1990) computed the reduction of fluxes due to CO_2 based on the pressure scaling of (3.5) and ignoring CO_2 absorption in the weak bands at 6400 cm^{-1} and 7000 cm^{-1} and in the strong 2300 cm^{-1} band, where the insolation is weak. A deficiency of this approach is that the heating rate in the upper stratosphere was greatly underestimated due to the use of the pressure scaling. To demonstrate the importance of the CO_2 heating in the stratosphere, Figure 2 shows the line-by-line calculated heating rate profile (solid curve) in the spectral region 2200-2400 cm^{-1} and 3500-3760 cm^{-1}, where CO_2 absorption is strong. The heating rate increases from 1 °C day^{-1} at 0.1 hPa to ~ 4.5 °C day^{-1} at 0.01 hPa . For an atmospheric model which extends to the middle atmosphere, it is desirable to include this large heating.

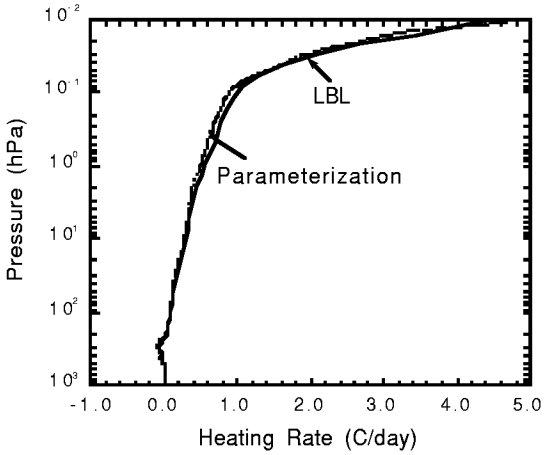

Figure 2. The effect of CO_2 absorption in the spectral regions 2200-2400 cm^{-1} and 3500-3760 cm^{-1} on the solar heating. Overlapping with water vapor absorption is included in the calculations of CO_2 effect. The solid curve is line-by-line calculations, and the dashed curve is the parameterization using the precomputed table of $\Delta F(\rho_c / \mu_o, p)$ given by (3.19). The CO_2 concentration is set to 350 ppmv, and the solar zenith angle is set to 60°.

In the 2200-2400 cm^{-1} band, water vapor absorption is negligible; whereas in the 3500-3760 cm^{-1} band, water vapor absorption is very strong in the troposphere but weak in the stratosphere, and the effect of CO_2 on the tropospheric heating can be neglected. It follows that the absorption due to CO_2 in these spectral regions is not sensitive to water vapor amount, and an average water vapor path can be used in the parameterization for the flux reduction due to CO_2. By using a fixed water vapor path, the CO_2-induced flux reduction at a given pressure level becomes a function only of the CO_2 concentration and the solar zenith angle,

$$\Delta F(\rho_c / \mu_o, p) = \int e^{-\tau_w(p)} \left[1 - e^{-\tau_c(\rho_c/\mu_o, p)}\right] S_\nu d\nu \tag{3.19}$$

where

$$\tau_w(p) = \frac{1}{\bar{\mu} g} \int_0^p k_\nu(p) q(p) dp \tag{3.20}$$

$$\tau_c(\rho_c / \mu_o, p) = \frac{\rho_c}{\mu_o g} \int_0^p \gamma_\nu(p) dp \tag{3.21}$$

k and γ are the absorption coefficients of water vapor and CO_2, ρ_c is the CO_2 concentration independent of space, q is the water vapor mixing ratio of a typical midlatitude summer atmosphere, μ_o is the cosine of the solar zenith angle, and $\bar{\mu}$ is taken to be 0.5. Using the line-by-line method, a table for $\Delta F(\rho_c / \mu_o, p)$ normalized by S_o is precomputed for ρ_c / μ_o ranging from 250 ppmv to 3300 ppmv and p ranging from 0.01 hPa to 1000 hPa. The CO_2 heating in 2200-2400 cm^{-1} and 3500-3760 cm^{-1} derived from the precomputed table of $\Delta F(\rho_c / \mu_o, p)$ is shown as the dashed curve of Figure 2. It agrees very well with the line-line-line calculations (solid curve).

For computing the CO_2 heating outside the strong bands at 2200-2400 cm^{-1} and 3500-3760 cm^{-1}, the approach of Chou (1990) is followed. Similar to (3.6) and (3.11), fluxes in the CO_2 bands are given by

$$F(w,u) = \int e^{-(k_\nu w + \gamma_\nu u)} S_\nu d\nu = S_o \sum_{i=1}^{n} \sum_{j=1}^{m} h_{i,j} e^{-(k_i w + \gamma_j u)} \tag{3.22}$$

where w and u are the scaled water vapor and CO_2 amounts, and $h_{i,j}$ is the flux-weighted k-distribution function with the absorption coefficients k_i and γ_j for the two absorbers, respectively. Equation (3.22) requires $(m \times n)$ sets of flux calculations, which becomes computationally very expensive when used in weather and climate models. Other approaches than the k-distribution method have to be used for efficient flux calculations when overlapping of absorption is involved.

The reduction in transmission due to CO_2 absorption can be expressed as

$$\Delta T(w,u) = \int e^{-k_\nu w} (1 - e^{-\gamma_\nu u}) S_\nu d\nu \Big/ \int S_\nu d\nu \tag{3.23}$$

Since $\Delta T(w,u)$ is a function only of w and u, it is pre-computed using the line-by-line method for large ranges of w and u encountered in the atmosphere. The integration is over the total solar spectrum. The absorption due to CO_2 in 2200-2400 cm^{-1} and 3500-3760 cm^{-1}, is excluded in computing $\Delta T(w,u)$. Fluxes in Band 10 are then simply computed from

$$F(w,u) = F(w) - S_o \Delta T(w,u), \tag{3.24}$$

where $F(w)$ is computed from (3.11).

4. MOLECULAR AND PARTICULATE SCATTERING

4.1 Rayleigh scattering

Rayleigh scattering decreases with decreasing wavenumber according to $\sim\nu^4$. Spectral values of Rayleigh scattering extinction coefficient are taken from a World Meteorological Organization report on atmospheric ozone (WMO, 1986). For each of Bands 1-10, a mean effective Rayleigh scattering coefficient is computed according to the same procedures as in the computation of the mean effective water vapor absorption coefficient in the PAR region, (3.13). The Rayleigh scattering coefficients for Bands 1-10 are given in Table 3.

4.2. Cloud and rain single-scattering properties

Radiation routines for atmospheric models usually use only a few broad spectral bands, with effective optical properties parameterized for each band. The single-scattering co-albedo, $1-\omega_\nu$, varies by several orders of magnitude in the solar spectrum. It is, therefore, difficult to derive an effective ω for a broad spectral band that can be applied to both strong and weak absorption situations. There are a number of approaches to deriving ω. Slingo and Schrecker (1982) derived ω by weighting ω_ν with the solar insolation and linearly averaging over a spectral band. Espinoza and Harshvardhan (1996) used a square-root approximation to derive ω. Fu (1996) used a mix of linear and logarithmic averaging depending on the strength of absorption in a given spectral band. The absorption of solar radiation by clouds depends not only on ω_ν but also on water vapor and cloud ice/water amounts. It is clear that no optimal method has been found for deriving ω over a broad band. It can only be empirically determined based on the amounts of cloud particles and

water vapor encountered in the Earth's atmosphere. Let us define the linear and logarithmic averaging over a band as

$$(1-\omega') = \sum(1-\omega_\nu)\beta_\nu S_\nu \Delta\nu / \sum \beta_\nu S_\nu \Delta\nu \tag{4.1}$$

$$\log(1-\omega'') = \sum \log(1-\omega_\nu)\beta_\nu S_\nu \Delta\nu / \sum \beta_\nu S_\nu \Delta\nu \tag{4.2}$$

where S_ν is the solar insolation at the top of the atmosphere (TOA), and $\Delta\nu$ is a narrow spectral interval where optical properties can be treated as constants. The effective mean single-scattering co-albedo of a band is then computed from

$$(1-\omega) = \eta(1-\omega') + (1-\eta)(1-\omega'') \tag{4.3}$$

where η is the weight ranging from 0 to 1. The weight η should be close to 1 for the spectral bands with weak absorption and should decrease as absorption increases. Chou et al. (1997) determined empirically the weight in the various spectral bands that minimize errors in flux calculations.

Compared to ω_ν, the extinction coefficient (β_ν) and the asymmetry factor (g_ν) vary rather smoothly with ν. Their effective mean values over a wide spectral band can be accurately approximated by

$$\beta = \sum \beta_\nu S_\nu \Delta\nu / \sum S_\nu \Delta\nu \tag{4.4}$$

$$g = \sum g_\nu \omega_\nu \beta_\nu S_\nu \Delta\nu / \sum \omega_\nu \beta_\nu S_\nu \Delta\nu \tag{4.5}$$

Theoretical considerations and radiative transfer calculations have shown that cloud single-scattering properties are not significantly affected by details of the particle size distribution and can be adequately parameterized as functions of the effective particle size (Fu, 1996; Hu and Stamnes, 1993; Tsay et al., 1989). Following Slingo and Schrecker (1982), we parameterize the single-scattering properties for a broad spectral band by

$$\beta = a_o + a_1 / r_e \tag{4.6}$$

$$1-\omega = b_o + b_1 r_e + b_2 r_e^{\,2} \tag{4.7}$$

$$g = c_o + c_1 r_e + c_2 r_e^{\,2} \tag{4.8}$$

where a, b, and c are regression coefficients, and r_e is the effective particle size defined to be proportional to the ratio of the total volume of cloud particles to the total cross-sectional area, A_c of cloud particles. For spherical water droplets, the effective size is given by

$$r_w = \int_0^\infty r^3 n(r)dr \Big/ \int_0^\infty r^2 n(r)dr = \frac{3}{4\rho_w}\frac{C}{A_c} \tag{4.9}$$

where ρ_w is the density of water. For hexagonal ice crystals randomly oriented in space, the effective size is shown by Fu (1996) to be

$$r_i = \frac{2\sqrt{3}}{3\rho_i}\frac{C}{A_c} \tag{4.10}$$

where ρ_i is the density of ice, and C is the cloud water/ice mass concentration per unit volume. The cloud optical thickness, τ_c, is then given by

$$\tau_c = \beta C z \tag{4.11}$$

where z is the geometric thickness of a cloud layer.

The size, shape, and refractive indices are different for ice crystals and water droplets. The extinction coefficient of ice clouds is smaller than that of water clouds because ice crystals are much larger than water droplets. The single-scattering albedo and asymmetry factor of ice clouds and water clouds are also different. Therefore, we parameterize the single-scattering properties separately for ice and water clouds.

The spectral data ω_ν, β_ν, and g_ν calculated by Fu (1996) for ice clouds and by Tsay et al. (1989) for water clouds are used to derive ω, β, and g from (4.1)-(4.5) as functions of phase and size. By assuming hexagonal ice crystals randomly oriented in space, Fu (1996) computed the single-scattering parameters of ice clouds using the improved ray-tracing method of Yang and Liou (1995). A total of 28 size distributions derived from *in situ* aircraft measurements were used in the calculations, which included samples from the FIRE (First ISCCP Regional Experiment) and CEPEX (Central Equatorial Pacific Experiment) field campaigns. The mean effective size of ice crystals, r_i, ranges from 20 μm to 130 μm. For water clouds, the single-scattering parameters of 5 water clouds were computed by Tsay et al.

(1989) from the Mie theory assuming spherical droplets and a log-normal size distribution. The effective radius of water droplets, r_w, ranges from 4 μm to 20 μm.

Figures 3-5 show the results of regression using (4.6)-(4.8). The coefficients a, b, and c are shown in Tables 4-6, respectively. It can be seen in Figure 3 that the extinction coefficient varies weakly with spectral band but strongly with particle size. For large particles, it is independent of wavelength for both water and ice clouds. The results shown in Figure 3 for ice clouds are indistinguishable among the four bands. Due to a large particle size, the extinction coefficient of ice clouds is significantly smaller than that of water clouds. It is interesting to note that in spite of a large difference in the particle size distribution, the ice particle extinction coefficients for the 28 clouds nearly fall onto a single curve of (4.6). Figure 4 shows the single-scattering co-albedo of Bands 9-11. The single-scattering co-albedo of Band 1-8 is very small ($<10^{-5}$) and is set to 0. For a given particle size, the single-scattering co-albedo varies by 3 orders of magnitude among the three IR bands. For a given spectral band, it is ~ 8 times larger for ice clouds than for water clouds. The asymmetry factor, shown in Figure 5, varies between 0.78 and 0.94 for different bands and particle sizes. Since the shape of size distribution has little effect on the single-scattering properties (Hu and Stamnes, 1993; Slingo and Schrecker, 1982), the results shown in Figures 3-5 should be representative for a wide range of clouds with various particle size distributions.

For rain drops, a single drop-size distribution is used to compute the spectral distribution of the single-scattering properties. Fu et al. (1995) used a truncated constant-slope gamma function (Manton and Cotton, 1977) with a minimum size of 60 μm, a maximum size of 1800 μm, and a mean effective size of 162 μm to compute the single-scattering properties. The mean effective extinction coefficient, single-scattering co-albedo, and asymmetry factor for the 11 spectral bands are shown in Tables 4-6. They are applied to all other drop-size distributions. The results are provided to us by Prof. Qiang Fu

4.3. Aerosol single-scattering properties

The aerosol optical thickness, single-scattering albedo, and asymmetry factor are not parameterized. They need to be specified as functions of height and spectral band for input to the radiation routine.

Table 4. Coefficients a_o and a_1 of the parameterization, Equation (4.6), for the cloud extinction coefficient. The units of a_o and a_1 are, respectively, $m^2\ g^{-1}$ and $m^2\ g^{-1}\ \mu m$.

Spectral Band	Ice Cloud		Water Cloud		Rain	
	a_o	a_1	a_o	a_1	a_o	a_1
1-8	3.33e-4	2.52	-6.59e-3	1.65	3.07 e-3	0.0
9	3.33e-4	2.52	-1.01e-2	1.72	3.07 e-3	0.0
10	3.33e-4	2.52	-1.66e-2	1.85	3.07 e-3	0.0
11	3.33e-4	2.52	-3.39e-2	2.16	3.07 e-3	0.0

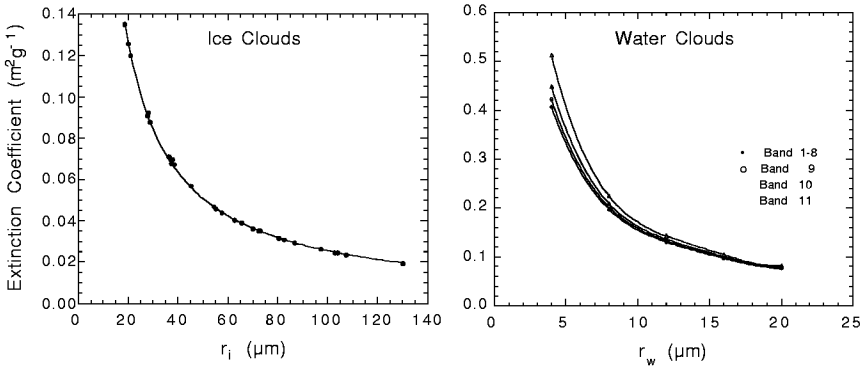

Figure 3. The extinction coefficient of ice and water clouds as a function of the effective particle size. r_i and r_w are, respectively, the effective size of ice and water particles. The data points are derived from Equation (4.4), whereas the curves are the regression using Equation (4.6).

Table 5. Coefficients b_0, b_1, and b_2 of the parameterization, Equation (4.7), for the cloud single-scattering co-albedo. The units of b_1 and b_2 are, respectively, μm^{-1} and μm^{-2}.

Spectral Band	Ice Cloud			Water Cloud			Rain		
	b_0	b_1	b_2	b_0	b_1	b_2	b_0	b_1	b_2
1-8	0.0	0.0	0.0	0.0	0.0	0.0	0.0	0.0	0.0
9	-2.60e-6	7.46e-6	0.0	7.15e-8	8.45e-6	-4.15e-8	0.029	0.0	0.0
10	2.15e-3	7.37e-4	-1.34e-6	-1.99e-4	8.88e-4	-6.50e-6	0.342	0.0	0.0
11	8.94e-2	2.99e-3	-1.04e-5	1.21e-2	1.79e-2	-3.69e-4	0.466	0.0	0.0

Table 6. Coefficients c_0, c_1, and c_2 of the parameterization, Equation (4.8), for the cloud asymmetry factor. The units of c_1 and c_2 are, respectively, μm^{-1} and μm^{-2}.

Spectral Band	Ice Cloud			Water Cloud			Rain		
	c_0	c_1	c_2	c_0	c_1	c_2	c_0	c_1	c_2
1-8	7.46e-1	1.05e-3	-2.64e-6	8.26e-1	5.29e-3	-1.49e-4	0.883	0.0	0.0
9	7.49e-1	1.20e-3	-3.67e-6	7.94e-1	8.32e-3	-2.33e-4	0.891	0.0	0.0
10	7.61e-1	1.42e-3	-3.96e-6	7.45e-1	1.37e-2	-3.82e-4	0.948	0.0	0.0
11	8.41e-1	1.26e-3	-3.85e-6	8.35e-1	2.57e-3	5.52e-5	0.971	0.0	0.0

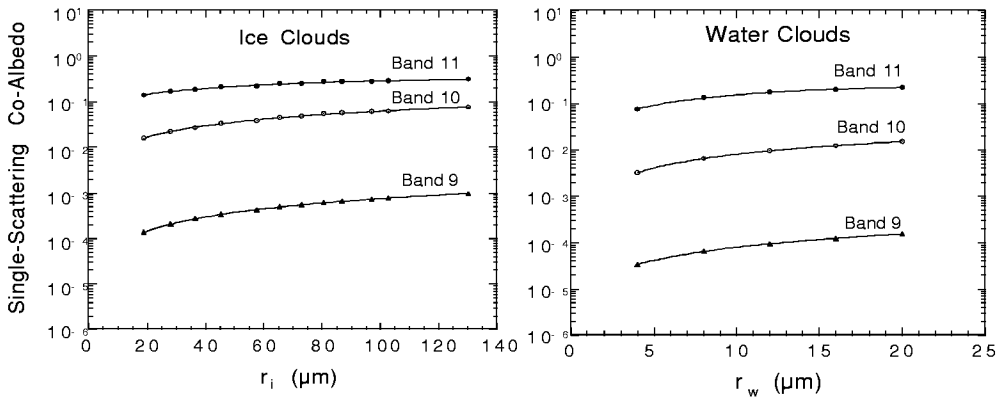

Figure 4. The single-scattering co-albedo of ice and water clouds as a function of the effective particle size. r_i and r_w are, respectively, the effective size of ice and water particles. The data points are derived from Equations. (4.1)-(4.3), whereas the curves are the regression using Equation (4.7).

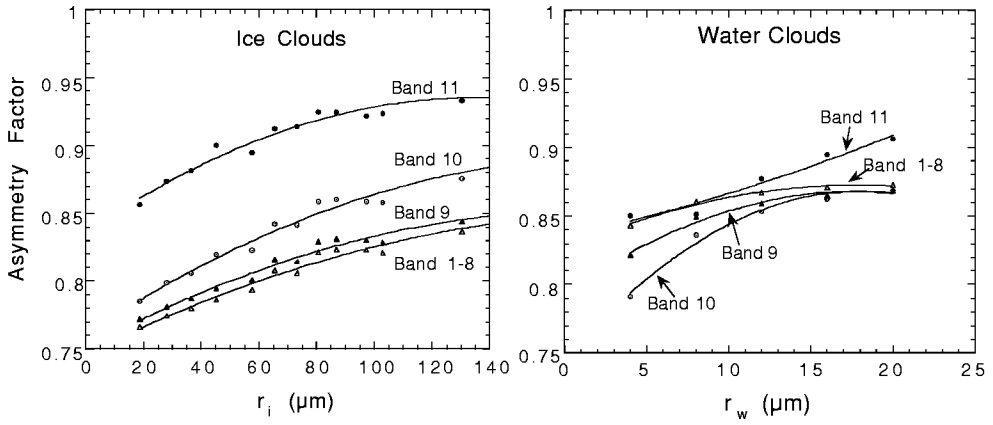

Figure 5. The asymmetry factor of ice and water clouds as a function of the effective particle size. r_i and r_w are, respectively, the effective size of ice and water particles. The data points are derived from Equation (4.5), whereas the curves are the regression using Equation (4.8).

5. SURFACE ALBEDO

The surface albedo is an input parameter and is separately specified for the UV and PAR region (Bands 1-8) and the infrared (Bands 9-11). It is also separately specified for direct and diffuse fluxes. Therefore, a set of four surface albedos must be specified as input to the radiation routine.

6. FLUX CALCULATIONS

As mentioned in the previous sections, single values of the gaseous absorption coefficients and particle single-scattering properties are used for each of the 11 bands, except for the water vapor absorption coefficient in the IR region (Bands 9-11) where the k-distribution method is used. Therefore, one set of fluxes in the atmosphere and at the surface are computed for each band in the UV and visible regions (Bands 1-8), and 10 sets of fluxes corresponding to 10 values of the water vapor absorption coefficient are computed for each of the IR bands (Bands 9-11). Reflectivities and transmissivities of each atmospheric layer are first computed using the δ-Eddington approximation (Joseph et al., 1976), fluxes are then computed by using a two-stream adding method for a composite of layers. The total flux at each pressure level and at the surface is the weighted sum of these fluxes,

$$F(p) = \sum_{i=1}^{38} \psi_i F_i(p) \tag{6.1}$$

where ψ_i is the fraction of extraterrestrial solar flux contained either in one of the first 8 bands (S / S_o given in Table 3) or in one of the 30 k-intervals in the three IR bands (h given in Table 2). The sum of ψ_i is 1.

6.1 Layer optical properties

For each atmospheric layer and spectral band, the effective optical thickness, single-scattering albedo, and asymmetry factor are computed from

$$\tau = \sum_i \tau_i \tag{6.2}$$

$$\overline{\omega} = \sum_i \omega_i \tau_i \Big/ \sum_i \tau_i \tag{6.3}$$

$$\overline{g} = \sum_i g_i \omega_i \tau_i \Big/ \sum_i \omega_i \tau_i \tag{6.4}$$

where the summation is over all gases and particles, i. They include ozone, water vapor, clouds, aerosols, and atmospheric gases (Rayleigh scattering). The single-scattering albedo is set to 1 for cloud scattering in the UV and visible regions (Bands 1-8) and for Rayleigh scattering in all bands, whereas it is set to 0 for ozone and water vapor. Cloud ice and water particles are allowed to mix in a layer. Absorption due to CO_2 and O_2 is treated differently and is addressed in Section 6.4

6.2 Layer reflectivities and transmissivities

The transmissivity T and reflectivity R of a layer illuminated by a direct beam are computed from the δ-Eddington approximation as a function of μ_o and the optical properties τ, $\overline{\omega}$, and $\overline{g}$ defined by (6.2)-(6.4). King and Harshvardhan (1986) have shown that errors in transmissivity and reflectivity induced by this approximation are ~5%. For diffuse insolation, the transmissivity $\overline{T}$ and reflectivity $\overline{R}$ are also computed from the δ-Eddington approximation but incident angles are approximated by a single value of 53°,

$$\overline{R} \sim R(\overline{\mu}) \tag{6.5}$$

$$\overline{T} \sim T(\overline{\mu}) \tag{6.6}$$

where $\overline{\mu}$=cos(53°).

To evaluate the errors induced by this approximation, we use the discrete-ordinate multiple-scattering algorithm of Stamnes et al. (1988) to compute the transmissivity and reflectivity of a layer for various incident angles. The diffuse transmissivity and reflectivity are derived by averaging the direct-beam transmissivity and reflectivity over 2π solid angles,

$$\overline{R} = 2\int_0^1 R(\mu)\mu d\mu \tag{6.7}$$

$$\overline{T} = 2\int_0^1 T(\mu)\mu d\mu \tag{6.8}$$

where μ is the cosine of the incident angle depart from the vertical. Errors induced by (6.5) and (6.6) are shown in Figure 6 for large ranges of the optical thickness and single-scattering co-albedo. Figure 6 shows that the approximation introduces an error < 0.02 in both the reflectance and transmittance for wide ranges of the optical thickness and the single-scattering

albedo, and an asymmetry factor of 0.8. For other values of the asymmetry factor, results are similar.

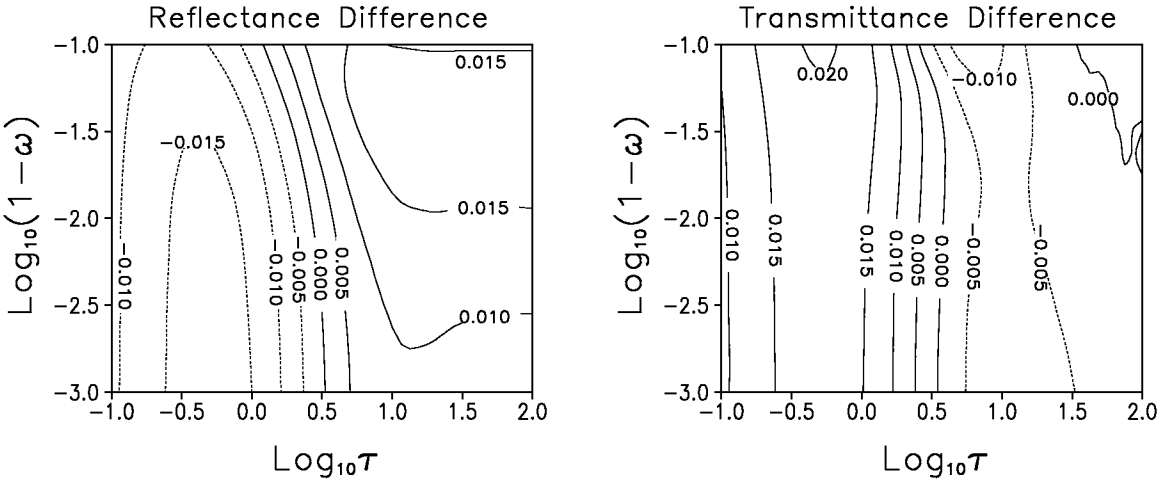

Figure 6. The left panel is the diffuse reflectivity computed from (6.5) minus that computed from (6.7). The right panel is the diffuse transmissivity computed from (6.6) minus that computed from (6.8). The cloud asymmetry factor is set to 0.85.

6.3 Two-stream adding approximation and flux calculations

Let us consider a layer divided into an upper sublayer a and a lower sublayer b. The direct-beam transmissivity T, the direct-beam reflectivity R, the diffuse transmissivity $\overline{T}$, and the diffuse reflectivity $\overline{R}$ of each of the two sublayers are computed from the δ-Eddington approximation. By separating the direct and diffuse components of the radiation, the reflectivity and transmissivity of the layer when illuminated by direct radiation can be computed from (Chou, 1992)

$$R_{ab}(\mu_o) = R_a(\mu_o) + \overline{T}_a\left\{e^{-\tau_a/\mu_o}R_b(\mu_o) + \left[T_a(\mu_o) - e^{-\tau_a/\mu_o}\right]\overline{R}_b\right\} / (1 - \overline{R}_a\overline{R}_b) \tag{6.9}$$

$$T_{ab}(\mu_o) = e^{-\tau_a/\mu_o}T_b(\mu_o) + \overline{T}_b\left\{e^{-\tau_a/\mu_o}\overline{R}_aR_b(\mu_o) + \left[T_a(\mu_o) - e^{-\tau_a/\mu_o}\right]\right\} / (1 - \overline{R}_a\overline{R}_b) \tag{6.10}$$

where $T(\mu_o)$, $e^{-\tau/\mu_o}$, and $T(\mu_o)-e^{-\tau/\mu_o}$ are the total, direct, and diffuse transmissivities, respectively. The subscripts a and b denote the upper layer and the lower layer.

The reflectivity of the layer when illuminated by diffuse radiation from above, $\overline{R}_{ab}$, is generally different from that when illuminated from below, $\overline{\overline{R}}_{ab}$. They can be computed from

$$\overline{R}_{ab}=\overline{R}_a+\overline{T}_a\overline{R}_b\overline{T}_a/(1-\overline{R}_a\overline{R}_b) \tag{6.11}$$

$$\overline{\overline{R}}_{ab}=\overline{R}_b+\overline{T}_b\overline{R}_a\overline{T}_b/(1-\overline{R}_a\overline{R}_b) \tag{6.12}$$

where the overbar and double-overbar denote illumination from above and below the layer, respectively.

When illuminated by a direct beam radiation at the top of the layer, the reflectivity, $R^{\uparrow}$, and the transmissivity, $T^{\downarrow}$, at the interface of the sublayers a and b are given by

$$R^{\uparrow}=\left\{e^{-\tau_a/\mu_o}R_b(\mu_o)+\left[T_a(\mu_o)-e^{-\tau_a/\mu_o}\right]\overline{R}_b\right\}/(1-\overline{R}_a\overline{R}_b) \tag{6.13}$$

$$T^{\downarrow}=e^{-\tau_a/\mu_o}+\left\{e^{-\tau_a/\mu_o}\overline{R}_aR_b(\mu_o)+\left[T_a(\mu_o)-e^{-\tau_a/\mu_o}\right]\right\}/(1-\overline{R}_a\overline{R}_b) \tag{6.14}$$

It follows from (6.13) and (6.14) that the upward and downward fluxes at the level $i+1/2$ (the lower boundary of the layer i in the atmosphere) can be computed from

$$F_{i+1/2}\uparrow=S\left\{e^{-\tau_{1,i}/\mu_o}R_{i+1,k}(\mu_o)+\left[T_{1,i}(\mu_o)-e^{-\tau_{1,i}/\mu_o}\right]\overline{R}_{i+1,k}\right\}/ \tag{6.15}$$
$$(1-\overline{\overline{R}}_{1,i}\overline{R}_{i+1,k})$$

$$F_{i+1/2}\downarrow=Se^{-\tau_{1,i}/\mu_o}+S\left\{e^{-\tau_{1,i}/\mu_o}\overline{\overline{R}}_{1,i}R_{i+1,k}(\mu_o)+\left[T_{1,i}(\mu_o)-e^{-\tau_{1,i}/\mu_o}\right]\right\}/ \tag{6.16}$$
$$(1-\overline{\overline{R}}_{1,i}\overline{R}_{i+1,k})$$

where S is the insolation at the top of the atmosphere, the index k denotes the surface, and the subscripts (1, i) and ($i+1$, k) denote the regions above and below the level $i+1/2$, respectively. The transmission $T_{1,i}$ and reflection $\overline{\overline{R}}_{1,i}$ of the region above the level are computed by adding layers from the top of the atmosphere to the layer i using (6.10) and (6.12) according to the procedures given in Lacis and Hansen (1974). Similarly, the

reflectivities $R_{i+1.k}$ and $\overline{R}_{i+1,k}$ are computed by adding layers from the surface up to the layer $i+1$ using (6.9) and (6.11).

Fluxes are computed for each of the 8 bands in the UV and PAR regions and for each of the 30 k-intervals in the IR bands. Total fluxes are the sum of these fluxes given by (6.1).

6.4 Flux reduction due to CO_2 and O_2

The reduction of the downward flux due to O_2 and CO_2 in clear sky conditions, $\Delta F^{\downarrow}_{clr}$, is computed from (3.18), (3.19), and (3.24). To simplify flux calculations in cloudy conditions, the effect of O_2 and CO_2 on solar heating is approximated by

$$\Delta F^{\downarrow}_{cld}(p) = \Delta F^{\downarrow}_{clr}(p), \qquad \text{for } p \le p_c \tag{6.17}$$

$$\Delta F^{\downarrow}_{cld}(p) = \Delta F^{\downarrow}_{clr}(p)\left[\frac{F^{net}_{cld}(p)}{F^{net}_{clr}(p)}\right] \qquad \text{for } p > p_c \tag{6.18}$$

where F^{net} is the total net downward flux without O_2 and CO_2 absorption, and p_c is the cloud-top pressure.

7. CLOUD OVERLAPPING

Clouds could occur at various heights with different fractional cover and optical properties. Nearly all radiative transfer algorithms used in atmospheric models apply only to a plane-parallel (i.e. horizontally homogeneous) atmosphere. Horizontal inhomogeneity is not allowed. A straightforward approach to dealing with a partial cloudiness situation is to divide a region into sections. Within each section, an atmospheric layer is either free of clouds or filled totally with a homogeneous cloud. Radiative fluxes are then computed for each section, and the total solar heating is the sum of all sections weighted by their fractional cover. Depending upon the number of cloud layers and the way these clouds overlap, computational costs of this approach could be huge. To simplify the computations, a cloud that partially fills a layer is usually smeared over the entire layer, and the optical thickness, τ, is adjusted by a factor dependent on the fractional cloud cover. As demonstrated by a number of studies (e.g. Harshvardhan and Randall 1985; Cahalan et al., 1994), the effect of τ on radiation is highly nonlinear, and it is not appropriate to scale τ (or cloud water path) linearly by cloud cover. In the NCAR (National Center for Atmospheric Research)

community climate model CCM, the optical thickness is scaled by $f^{1.5}$, where f is the fractional cloud cover (Briegleb, 1992). In the Goddard GCM, Sud et al. (1993) scaled the optical thickness by inverting a simple reflection function for clouds when illuminated by diffuse radiation and assuming no absorption by clouds. As can be expected, the effective optical thickness corresponding to a cloud smeared to cover the entire layer is a function of τ, f, and the solar zenith angle, as well as whether scaling is based on reflection or absorption. Scaling of τ is further complicated by the ways that clouds in various layers overlap.

7.1. Maximum-random overlapping

Treatments of cloud overlapping in climate studies differ from model to model. In our radiation parameterization, a combination of maximum and random cloud overlapping scheme similar to that of Geleyn and Hollingsworth (1979) is used (Chou et al., 1997). Clouds are identified as high, middle, or low separated roughly by the 400-hPa and 700-hPa levels. Cloud layers close to each other are likely to be related; therefore, cloud layers in each of the three height groups are assumed to be maximally overlapped (left panel of Figure 7), whereas overlapping among the three groups is assumed to be random. Scaling of τ is applied only to the maximally-overlapped clouds within each of the three height groups, but not to the randomly-overlapped clouds among different height groups (right panel of Figure 7). Within each height group, clouds are smeared over the extent of the maximum cloud amount, f_m, of that height group by scaling τ (right panel of Figure 7). By assuming random overlapping of clouds among different height groups, the atmosphere is then divided into 2^n sections, where $n \le 3$ is the number of height groups containing clouds (right panel of Figure 7). Within each section, a layer is either totally cloud-filled or cloud-free. Fluxes are first computed for each section and then summed over all sections weighted by the fractional cover of the individual sections.

As examples, the fractional cover of the clear section, A_{clr}, is computed from

$$A_{clr} = (1 - f_{m,1})(1 - f_{m,2})(1 - f_{m,3}) \tag{7.1}$$

where the subscripts 1, 2, and 3 denotes the upper, middle, and lower cloud groups, respectively. Similarly, the fractional cover of the section with only high clouds is computed from

$$A = f_{m,1}(1 - f_{m,2})(1 - f_{m,3}) \tag{7.2}$$

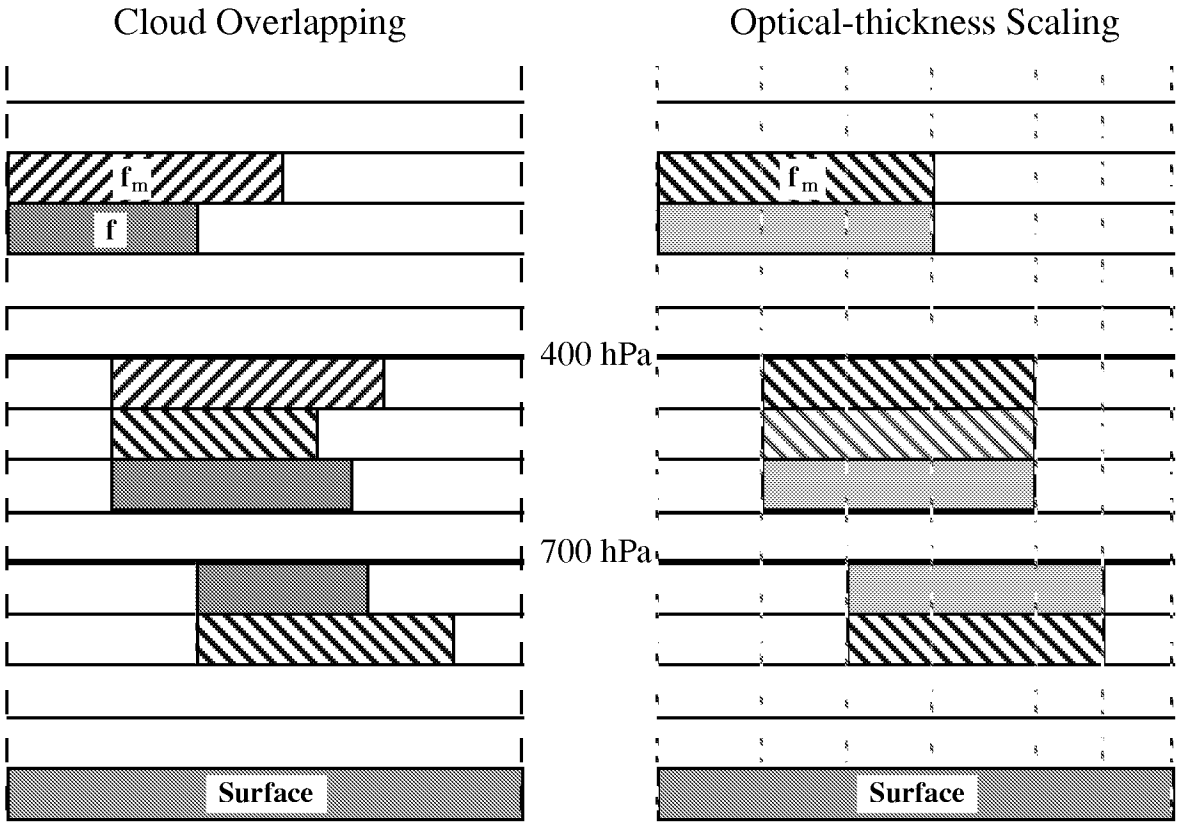

Figure 7. The maximum-random cloud-overlapping scheme. Clouds are identified as high, middle, and low separated roughly by the 400 hPa and 700 hPa levels. Clouds are assumed maximally overlapped within each height group and randomly overlapped among different height groups (left panel). Scaling of the optical thickness applies only to the maximally-overlapped cloud layers (right panel).

7.2. Scaling of optical thickness

Cloud optical-thickness scaling used to "smear" the clouds to f_m within each height group is based on the maximum-random cloud overlapping assumption shown in Figure 7. To simplify the scaling of τ, we assume that reflection is more important to climate than absorption, since the former affects the total heating of the earth-atmosphere system, but the latter only redistributes the heating within the atmosphere, as well as between the atmosphere and the surface. As stated in Sections 6.2 and 6.3, our radiation algorithm requires calculations of reflection/transmission of a cloud layer separately for direct and diffuse radiation. By smearing cloud cover over the extent of the maximum cloud cover of respective height-group, the optical thickness of a cloud layer is scaled by factors χ_s and $\overline{\chi}_s$,

$$\tau_b = \chi_s \tau \qquad \text{for direct radiation} \qquad (7.3)$$

$$\tau_f = \overline{\chi}_s \tau \qquad \text{for diffuse radiation} \qquad (7.4)$$

so that albedos of the layer remain the same before and after scaling,

$$R(\tau_b, r_e, \mu_o) = f' R(\tau, r_e, \mu_o) \qquad \text{for direct radiation} \qquad (7.5)$$

$$\overline{R}(\tau_f, r_e) = f' \overline{R}(\tau, r_e) \qquad \text{for diffuse radiation} \qquad (7.6)$$

where μ_o is the consine of the solar zenith angle, R is the albedo averaged over the entire solar spectrum for direct incident radiation, $\overline{R}$ is the albedo for diffuse incident radiation given by

$$\overline{R}(\tau, r_e) = 2\int_0^1 R(\tau, r_e, \mu)\mu \, d\mu \qquad (7.7)$$

f' is the normalized cloud cover given by

$$f' = f / f_m \qquad (7.8)$$

and μ is the cosine of the zenith angle of an incident beam. Using the scaling of (7.3) and (7.4), a layer with a fractional cloud cover f and an optical thickness τ is reduced to a layer with a fractional cloud cover f_m and an equivalent optical thickness τ_b for direct radiation and τ_f for diffuse radiation. It is noted that the scaling is a function of the incident angle, and that optical thickness is scaled separately for direct radiation and diffuse radiation.

Using values of r_e representative of the water and ice cloud samples used in Section 4.2, $\overline{\omega}$ and $\overline{g}$ are computed from (6.3) and (6.4) for the individual bands given in Table 1. Cloud albedos R and $\overline{R}$ averaged over the solar spectrum are computed using the discrete-ordinate multiple-scattering algorithm of Stamnes et al. (1988). The scaling functions χ_s and $\overline{\chi}_s$ are then derived from (7.3)-(7.6) by giving f', $R(\tau, r_e, \mu_o)$ and $\overline{R}(\tau, r_e)$. Sample calculations show that χ_s and $\overline{\chi}_s$ depend only weakly on r_e and the phase of cloud particles. Therefore, they are reduced to $\chi_s(f', \tau, \mu_o)$ and $\overline{\chi_s}(f', \tau)$ by taking the mean values of the scaling functions for various particle sizes and phases.

The above scaling ensures that the reflection of a cloud layer is the same before and after the scaling. However, errors are expected in the calculations of atmospheric and surface heating when there are other cloud layers present. In addition to the solar zenith angle, cloud cover, and optical thickness, an optimal cloud scaling should, in principle, also depend on the fractional cover and optical thickness of other cloud layers. This situation makes scaling of the optical thickness extremely difficult. To simplify the problem, we made simple adjustments to the scaling functions, χ_s and $\overline{\chi}_s$, so that errors in the fluxes at the TOA and the surface are minimized for the simplest cloud situation, which has two cloud layers in only one of the three height-groups. For the two-cloud situation, scaling is applied to the cloud with a smaller cloud cover (see right panel of Figure 7). It is noted that scaling is not required when there is only one cloud layer in a given height-group. The scaling functions are adjusted according to

$$\chi = \chi_s + (f - \chi_s)\delta \tag{7.9}$$

$$\overline{\chi} = \overline{\chi}_s + (f - \overline{\chi}_s)\overline{\delta}, \tag{7.10}$$

where δ and $\overline{\delta}$ are constants empirically (trial and error) chosen to minimize errors in the fluxes at the TOA and at the surface. The errors are defined as the differences between the flux computed with the scaling of τ and the flux computed with the sky divided into horizontally homogeneous sections (three sections in the two-cloud situation). The adjusted scaling functions preserve the shapes of χ_s and $\overline{\chi}_s$. The results for the scaling functions are saved as tables for later use. It is found that optimal values of δ and $\overline{\delta}$ are 0.2 and 0.3, respectively. The results for the scaling functions χ and $\overline{\chi}$ are shown in Figure 8. It can be

seen that $\chi(f', \tau, \mu_o) < f'$, and $\chi \to f'$ as $\tau \to 0$. For an optically thick cloud, χ and $\overline{\chi}$ are not sensitive to τ.

The scaling functions derived for the two-cloud situation is applied universally to all situations even if there are more than two cloud layers in a given height group. It implicitly assumes that, in a given height group, accurate scaling of τ is not critical if there are two cloud layers above.

With the sky divided into 2^n sections, fluxes are computed for each section. Instead of (6.1), the total flux is computed from

$$F(p) = \sum_{i=1}^{38} \psi_i \left[\sum_{j=1}^{N} A_j F_{i,j}(p) \right] \tag{7.11}$$

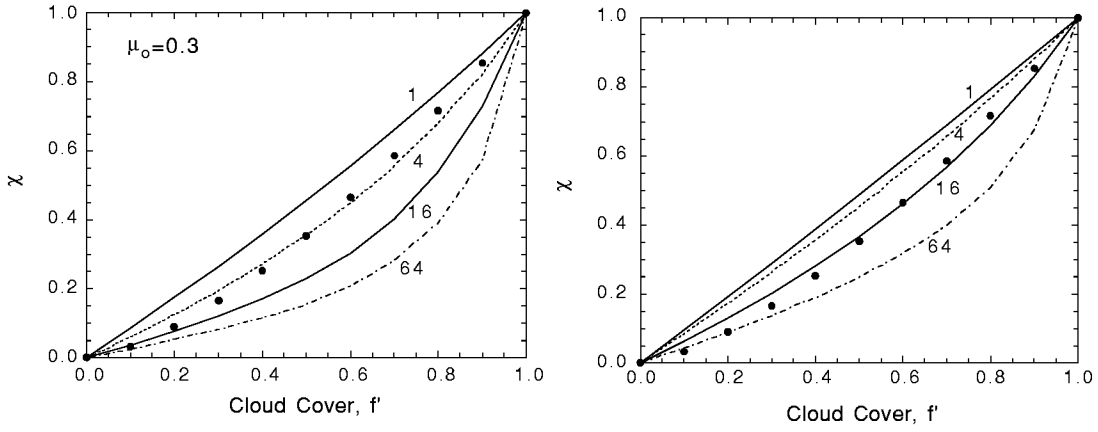

Figure 8. Scaling functions for the cloud optical-thickness, χ and $\overline{\chi}$, for direct (shown only for μ_o = 0.3) and diffuse radiation, respectively. The value of f' is the normalized cloud cover defined by (7.8). Numbers in the figure are the cloud optical thickness. The dots are $\chi = f'^{1.5}$ used in the NCAR CCM model (Briegleb, 1992).

where $N = 2^n$, and A_j is the fractional cover of the j^{th} section. The sums of $A_j's$ and $\psi_i's$ are both 1. It needs to compute the reflectivities and transmissivities of each of the

atmospheric layers only once but not N times. Depending upon the number of sections N, the total computing time is about three times larger than the computing time for a single section.

8. SAMPLE CALCULATIONS

8.1. Effect of absorption and scattering in minor bands

Concerned with the huge time required for computing radiative transfer in weather and climate models, solar heating in minor absorption bands has often been neglected. The individual contributions of these minor bands to the atmospheric heating is small, but collectively they are not negligible (Chou, 1999). The minor absorption and scattering which are often neglected include the absorption due to water vapor in the photosynthetically active radiation (PAR) spectral region (Band 8) and in the thermal infrared (1000-2600 cm^{-1}), the ozone absorption and Rayleigh scattering in the near infrared (Band 9), and O_2 and CO_2 absorption in wide spectral ranges. Ramaswamy and Freidenreich (1991) have shown the importance of the two minor water vapor regions. Table 7 shows the effects of these minor absorption and scattering bands on the surface solar heating for the typical midlatitude summer atmosphere with a CO_2 concentration of 350 ppmv, a solar zenith angle of 60°, and a surface albedo of 0. Using a spectral resolution of 0.002 cm^{-1} for water vapor, O_2, and CO_2, and 0.003 μm for O_3, the total effect of these minor bands is computed with the discrete-ordinary scattering algorithm. The surface solar heating is reduced by 17 W m^{-2}. The atmospheric solar heating increases by a similar amount, ~15 W m^{-2} (not shown) when these minor bands are included. This amounts to about 10% of the total atmospheric heating, which is not negligible in the solar heating calculations. The results of the parameterizations for these minor bands are also shown in the table, which are accurate compared to the detailed calculations.

8.2. Clear-sky fluxes and heating rates

Clear-sky fluxes and heating rates computed with the parameterization are validated with high spectral-resolution calculations. The results are shown in Table 8 for fluxes and Figure 9 for the heating rate. Calculations are for the mid-latitude summer atmosphere with a

Table 7. Effects of minor absorption and scattering on the downward surface solar flux from detailed high spectral-resolution calculations and parameterizations. Fluxes are computed for a typical mid-latitude summer atmosphere. The CO_2 concentration is set to 350 ppmv. The solar zenith angle and the surface albedo are set to 60° and zero, respectively. Units are W m^{-2}.

	Detailed Calculations	Parameterization
Water vapor in PAR	-2.53	-2.42
Ozone in near infrared*	-0.56	-0.54
Oxygen in near infrared*	-4.29	-4.18
CO_2 in middle infrared*	-3.30	-3.57
Rayleigh in near infrared*	-3.12	-2.82
H_2O in thermal infrared**	-3.09	***
Total	-16.89	

* Overlapping with water vapor absorption is included.

** 1000 cm^{-1}<ν<2600 cm^{-1}.

*** The effect cannot be assessed because a separate parameterization excluding the thermal infrared is not done.

CO_2 concentration of 350 ppmv. The solar zenith angle is set to 60°, and the surface albedo is set to 0.2. For the high resolution calculations, the spectral interval is chosen to be 0.003 μm for O_3 and 0.002 cm^{-1} for water vapor, O_2, and CO_2. Only the absorption due to water vapor, O_3, O_2, and CO_2 are included. Scattering due to clouds, aerosols, and gases are excluded.

Absorption of solar radiation in the atmosphere (ATM) and net downward fluxes at the top of the atmosphere (TOA) and the surface (SFC) are shown in Table 8 for different bands and the total spectrum. The parameterization introduces an error of <1% in the TOA and surface fluxes and the atmospheric heating. Figure 9 shows the heating rate as functions of the logarithm of pressure (left panel) and of pressure (right panel). The parameterization computes very accurately the heating rate below the 1-hPa level but with an error of 5% of the peak heating above. Most of the error is attributable to the use of the pressure scaling in the calculations of absorption due to water vapor, O_2, and CO_2.

Table 8. Net downward solar fluxes at the top of the atmosphere (TOA) and at the surface (SFC) and the radiation absorbed in the atmosphere (ATM) computed using high spectral resolution calculations and the parameterization. The atmosphere used is typical of a mid-latitude summer with a CO_2 concentration of 350 ppmv. The solar zenith angle and the surface albedo are set to 60° and 0.2, respectively. Calculations include the absorption due to water vapor, O_3, CO_2 and O_2 covering the spectral range from 0.175 μm to 10 μm. Scattering is excluded. Units are W m^{-2}.

	High Spectral-Resolution			Parameterization		
	TOA	SFC	ATM	TOA	SFC	ATM
Band 1-7	47.7	33.7	14.0	46.7	33.0	13.7
Band 8	217.7	203.2	14.5	218.0	203.9	14.1
Band 9	186.7	137.8	48.9	186.5	134.9	51.6
Band 10	101.5	51.0	50.5	100.3	51.7	48.6
Band 11	28.0	7.8	20.2	27.6	8.2	19.4
Total	581.5	433.3	148.2	579.1	431.7	147.4

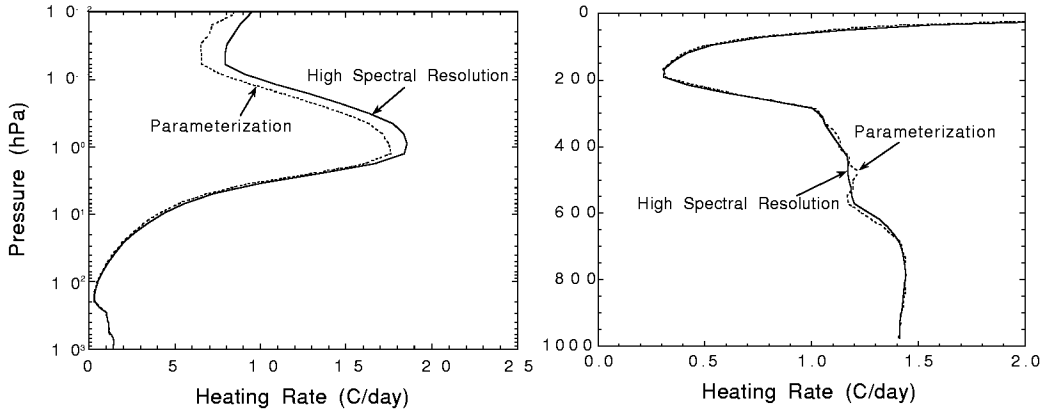

Figure 9. The heating rate profiles of a mid-latitude summer atmosphere computed with the line-by-line method (solid curves) and the parameterization (dashed curves). The heating is expressed as a function of the logarithm of pressure in the left panel and as a function of pressure in the right panel. The solar zenith angle is set to 60°, surface albedo is set to 0.2, and the CO_2 concentration is set to 350 ppmv. Absorption due to water vapor, O_3, O_2, and CO_2 are included. Scattering is excluded.

8.3. Cloudy-sky fluxes and heating rates

Fluxes and heating rates in a cloudy atmosphere derived from the parameterization and the detailed absorption and scattering calculations are compared. A deck of stratus cloud covering the entire sky is inserted between 800 hPa and 920 hPa. The effective radius of liquid cloud particles, r_w, is set to 12 μm, and the optical thickness in the 0.55 μm visible region, τ_{vis}, is set to 9.7. Based on results from Mie calculations for those r_w and τ_{vis}, the extinction coefficient in the visible region, β_{vis}, is 0.1303 g m^{-2}, and the total cloud water amount, Cz given by (4.11), is 74.4 g m^{-2}. The cloud layer is divided into 5 sublayers with a thickness of 24 hPa. For each sublayer, the cloud water amount is 14.9 g m^{-2}, and the optical thickness in the visible region is 1.94.

For the detailed calculations, the line-by-line method and the discrete-ordinate scattering algorithm are used. The spectral distributions of the cloud extinction coefficient, β_ν, the single-scattering albedo, ω_ν, and the asymmetry factor, g_ν, for r_w=12 μm are derived from Mie calculations. The spectral distribution of the optical thickness is scaled according to

$$\tau_\nu = \tau_{vis}\left(\frac{\beta_\nu}{\beta_{vis}}\right) \tag{8.1}$$

For the parameterization, the band-averaged cloud extinction coefficient, the single-scattering albedo, and the asymmetry factor are derived from (4.6)-(4.8), and the optical thickness is derived from (4.11). Fluxes are computed using the two-stream adding approximation given in Section 6.3.

Table 9 shows the net downward fluxes at the TOA and surface and the solar heating of the mid-latitude summer atmosphere using the detailed calculations and the parameterization. The solar zenith angle and the surface albedo are set to 60° and 0.2, respectively. The discrepancy between the two sets of calculations is very small in the surface flux and is ~2% in the total TOA flux. Figure 10 shows the heating rate profiles of the two sets of calculations. They agree very well both inside and outside the cloud.

Table 9. Same as Table 8 except scattering by gases and cloud is included. A deck of stratus cloud with an optical thickness of 9.7 in the visible region is located between 800 and 920 hPa. Units are W m^{-2}.

	Detailed Calculations			Parameterization		
	TOA	SFC	ATM	TOA	SFC	ATM
Band 1-8	138.7	105.8	32.9	137.8	107.3	30.5
Band 9	110.6	62.9	47.7	106.4	61.9	44.6
Band 10	78.5	17.9	60.6	74.1	18.5	55.7
Band 11	27.1	0.7	26.4	28.0	0.1	27.9
Total	354.9	187.2	167.7	346.4	186.9	159.6

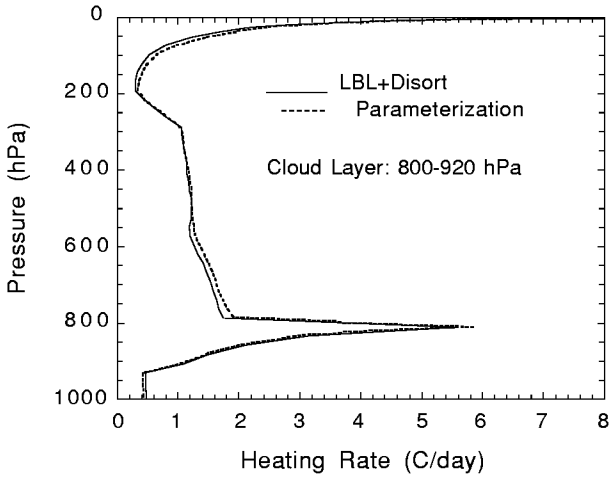

Figure 10. Same as Figure 9, except a cloud deck is inserted between 800 and 920 hPa. The cloud optical thickness is 9.7 in the visible region, and the effective radius of cloud liquid drops is 12 μm.

ACKNOWLEDGMENTS

This work was supported by the Global Atmospheric Modeling and Analysis Program, NASA/Office of Earth Science.

REFERENCES

Anderson, G. P., S. A. Clough, F. X. Kneizys, J. H. Chetwynd, and E. P. Shuttle, 1986: AFGL atmospheric constituent profiles (0-120 km), AFGL-TR-86-0110, 43 pp. [NTIS ADA175173]

Arking, A., and K. Grossman, 1972: The influence of line shape and band structure on temperatures in planetary atmospheres. *J. Atmos. Sci.*, **29**, 937-949.

Briegleb, B. P., 1992: Delta-Eddington approximation for solar radiation in the NCAR community climate model. *J. Geophy. Res.*, **97**, 7603-7612.

Cahalan, R. F., W. Ridgway, W. J. Wiscombe, and T. L. Bell, 1994: The albedo of stratocumulus clouds. *J. Atmos. Sci.*, **51**, 2434-2455.

Chou, M.-D., 1986: Atmospheric solar heating rate in the water vapor bands. *J Climate Appl. Meteor.*, **25**, 1532-1542.

Chou, M.-D., 1990: Parameterization for the absorption of solar radiation by O_2 and CO_2 with application to climate studies. *J. Climate*, **3**, 209-217.

Chou, M.-D., 1992: A solar radiation model for use in climate studies. *J. Atmos. Sci.*, **49**, 762-772.

Chou, M.-D., 1999: Atmospheric solar heating in minor absorption bands. *Terrest. Atmos. Ocean. Sci.*

Chou, M.-D., and K.-T. Lee, 1996: Parameterizations for the absorption of solar radiation by water vapor and ozone. *J. Atmos. Sci.*, **53**, 1203-1208.

Chou, M.-D., M. J. Suarez, C-H. Ho,' M. M.-H. Yan, and K. T. Lee, 1997: Parameterizations for cloud overlapping and shortwave single-scattering properties for use in general circulation and cloud ensemble models. *J. Climate*, **10**, 610-620.

Espinoza, R. C. Jr., and Harshvardhan, 1996: Parameterization of solar near-infrared radiative properties of cloudy layers. *J. Atmos. Sci.*, **53**, 1559-1568.

Fouquart, Y., B. Bonnel and V. Ramaswamy, 1991: Intercomparing shortwave radiation codes for climate studies. *J. Geophy. Res.*, **96**, 8955-8968.

Fu, Q., 1996: An accurate parameterization of the solar radiative properties of cirrus clouds for climate models. *J. Climate*, **9**, 2058-2082.

Fu, Q, and K.-N. Liou, 1992: On the correlated k-distribution method for radiative transfer in nonhomogeneous atmospheres. *J. Atmos. Sci.*, **49**, 2153-2170.

Fu, Q, S. K. Krueger, and K.-N. Liou, 1995: Interaction of radiation and convection in simulated tropical cloud clusters. *J. Atmos. Sci.*, **52**, 1310-1328.

Geleyn, J. F., and A. Hollingsworth, 1979: An economical analytical method for the computation of the interaction between scattering and line absorption of radiation. *Beitr. Phys. Atmos.*, **52**, 1-16

Goody, R. M., R. West, L. Chen, and D. Crisp, 1989: The correlated-k method for radiation calculation in nonhomogeneous atmospheres. *J. Quant. Spectrosc. Radiat. Transfer.*, **42**, 539-550.

Harshvardhan, and D. A. Randall, 1985: Comments on "The parameterization of radiation for numerical weather prediction and climate models." *Mon. Wea. Rev.*, **113**, 1832-1833.

Hu, Y. X., and K. Stamnes, 1993: An accurate parameterization of the radiative properties of water clouds suitable for use in climate models. *J. Climate*, **6**, 728-742.

Joseph, J. H., W. J. Wiscombe, and J. A. Weinman, 1976: The delta-Eddington approximation for radiative flux transfer. *J. Atmos. Sci.*, **33**, 2452-2459.

Kiehl, J. T., and T. Yamanouchi, 1985: A parameterization for solar absorption due to oxygen. *Tellus*, **37(B)**, 1-6.

Kiehl, J. T., J. J. Hack, and B. P. Briegleb, 1994: The simulated earth radiation budget of the National Center for Atmospheric Research community climate model CCM2 and comparisons with the Earth Radiation Budget Experiment (ERBE). *J. Geophy. Res.*, **99**, 20815-20827

King, M. D., and Harshvardhan, 1986: Comparative accuracy of selected multiple scattering approximations. *J. Atmos. Sci.*, **43**, 784-801.

Koster, R. D., and M. J. Suarez, 1995: Relative contribution of land and ocean processes to precipitation variability. *J. Geophy. Res.*, **100**, 13775-13790.

Lacis, A., and J. E. Hansen, 1974: A parameterization for the absorption of solar radiation in the Earth's atmosphere. *J. Atmos. Sci.*, **31**, 118-133.

Lacis, A., and V. Oinas, 1991: A description of the correlated k-distribution method for modeling nongray gaseous absorption, thermal emission, and multiple scattering in vertically inhomogeneous atmospheres. *J. Geophy. Res.*, **96**, 9027-9063.

Manton, M. J., and W. R. Cotton, 1977: Formulation of approximate equations for modeling moist deep convection on the mesoscale. Atmospheric Science Paper No. 266, Dept. of Atmospheric Science, Colorado State University, Fort Collins, CO, 62 pp.

Mlawer, E. J., S. J. Taubman, P. D. Brown, M. J. Iacono, and S. A. Clough, 1997: Radiative transfer for inhomogeneous atmospheres: RRTM, a validated correlated-k model for the longwave. *J. Geophy. Res.*, **102**, 16663-16682.

Ramaswamy, V., and S. M. Freidenreich, 1991: Solar radiative line-by-line determination of water vapor absorption and water cloud extinction in inhomogeneous atmospheres. *J. Geophy. Res.*, **96**, 9133-9157.

Rothman, L. S., R. R. Gamache, A. Barbe, A. Goldman, L. R. Brown, R. A. Toth, H. M. Pickett, R. L. Poynter, J.-M. Flaud, C. Camy-Peyret, A. Barbe, N. Husson, C. P. Rinsland, and M. A. Smith, 1987: The HITRAN data base: 1986 edition. *Appl. Opt.*, **26**, 4058-4097.

Slingo, A., and H. M. Schrecker, 1982: On the shortwave radiative properties of stratiform water clouds. *Q. J. R. Meteor. Soc.*, **108**, 407-426.

Stamnes, K., S.-C. Tsay, W. Wiscombe, and K. Jayaweera, 1988: Numerically stable algorithm for discrete-ordinate-method radiative transfer in multiple scattering and emitting layered media. *Appl. Opt.*, **27**, 2502-2509.

Sud, Y. C., W. C. Chao, and G. K. Walker, 1993: Dependence of rainfall on vegetation: Theoretical consideration, simulation experiments, observations, and inferences from simulated atmospheric soundings. *J. Arid Environ.*, **25**, 5-18.

Tao, W.-K., S. Long, J. Simpson, C.-H. Sui, B. Ferrier, and M.-D. Chou, 1996: Cloud-radiation mechanisms associated with a tropical and a mid-latitude squall line. *J. Atmos. Sci.*, **53**, 2624-2651.

Tsay, S. C., K. Stamnes, and K. Jayaweera, 1989: Radiative energy balance in the cloudy and hazy Arctic. *J. Atmos. Sci.*, **46**, 1002-1018.

Wang, W.-C., and P. B. Ryan, 1983: Overlapping effect of atmospheric H_2O, CO_2 and O_3 on the CO_2 radiative effect. *Tellus*, **35B**, 81-91.

World Meteorological Organization, 1986. *Atmospheric Ozone, Global Ozone Research and Monitoring Project.* Vol. **I**, Report No. **16**, 392 pp.

Yang, P., and K.-N. Liou, 1995: Light scattering by hexagonal ice crystals: Comparison of FDTD and geometric optics models. *J. Opt. Soc. Amer.*, **12**, 162-176.

REPORT DOCUMENTATION PAGE

Form Approved
OMB No. 0704-0188

1. AGENCY USE ONLY *(Leave blank)*	2. REPORT DATE	3. REPORT TYPE AND DATES COVERED
	June 1999	Technical Memorandum

4. TITLE AND SUBTITLE

Technical Report Series on Global Modeling and Data Assimilation
Volume 15—A Solar Radiation Parameterization for Atmospheric Studies

5. FUNDING NUMBERS

Code 913

6. AUTHOR(S)

Ming-Dah Chou and Max J. Suarez

7. PERFORMING ORGANIZATION NAME(S) AND ADDRESS (ES)

Climate and Radiation Branch
Goddard Space Flight Center
Greenbelt, Maryland 20771

8. PEFORMING ORGANIZATION REPORT NUMBER

99A01083

9. SPONSORING / MONITORING AGENCY NAME(S) AND ADDRESS (ES)

National Aeronautics and Space Administration
Washington, DC 20546-0001

10. SPONSORING / MONITORING AGENCY REPORT NUMBER

TM-1999-104606, Vol. 15

11. SUPPLEMENTARY NOTES

12a. DISTRIBUTION / AVAILABILITY STATEMENT

Unclassified–Unlimited
Subject Category: 46
Report available from the NASA Center for AeroSpace Information,
7121 Standard Drive, Hanover, MD 21076-1320. (301) 621-0390.

12b. DISTRIBUTION CODE

13. ABSTRACT *(Maximum 200 words)*

The solar radiation parameterization (CLIRAD-SW) developed at the Goddard Climate and Radiation Branch for application to atmospheric models are described. It includes the absorption by water vapor, O3, O2, CO2, clouds, and aerosols and the scattering by clouds, aerosols, and gases. Depending upon the nature of absorption, different approaches are applied to different absorbers. In the ultraviolet and visible regions, the spectrum is divided into 8 bands, and single O3 absorption coefficient and Rayleigh scattering coefficient are used for each band. In the infrared, the spectrum is divided into 3 bands, and the k-distribution method is applied for water vapor absorption. The flux reduction due to O2 is derived from a simple function, while the flux reduction due to CO2 is derived from precomputed tables. Cloud single-scattering properties are parameterized, separately for liquid drops and ice, as functions of water amount and effective particle size. A maximum-random approximation is adopted for the overlapping of clouds at different heights. Fluxes are computed using the Delta-Eddington approximation.

14. SUBJECT TERMS

Solar Radiation, Atmospheric Models, k-Distribution Method,
Delta-Eddington Approximation, Minor Absorption

15. NUMBER OF PAGES

40

16. PRICE CODE

17. SECURITY CLASSIFICATION OF REPORT	18. SECURITY CLASSIFICATION OF THIS PAGE	19. SECURITY CLASSIFICATION OF ABSTRACT	20. LIMITATION OF ABSTRACT
Unclassified	Unclassified	Unclassified	UL